ACS central science

Research Article

http://pubs.acs.org/journal/acscii

Nanoengineered Ultralight and Robust All-Metal Cathode for High-Capacity, Stable Lithium−Oxygen Batteries

Ji-Jing Xu, Zhi-Wen Chang, Yan-Bin Yin, and Xin-Bo Zhang*

State Key Laboratory of Rare Earth Resources Utilization, Changchun Institute of Applied Chemistry, Chinese Academy of Sciences, Changchun 130022, P. R. China

Supporting Information

ABSTRACT: The successful development of Li−O_2 battery technology depends on resolving the issue of cathode corrosion by the discharge product (Li_2O_2) and/or by the intermediates (LiO_2) generated during cell cycling. As an important step toward this goal, we report for the first time the nanoporous Ni with a nanoengineered AuNi alloy surface directly attached to Ni foam as a new all-metal cathode system. Compared with other noncarbonaceous cathodes, the Li−O_2 cell with an all-metal cathode is capable of operation with ultrahigh specific capacity (22,551 mAh g^{-1} at a current density of 1.0 A g^{-1}) and long-term life (286 cycles). Furthermore, compared with the popularly used carbon cathode, the new all-metal cathode is advantageous because it does not show measurable reactivity toward Li_2O_2 and/or LiO_2. As a result, extensive cyclability (40 cycles) with 87.7% Li_2O_2 formation and decomposition was obtained. These superior properties are explained by the enhanced solvation-mediated formation of the discharge products as well as the tailored properties of the all-metal cathode, including intrinsic chemical stability, high specific surface area, highly porous structure, high conductivity, and superior mechanical stability.

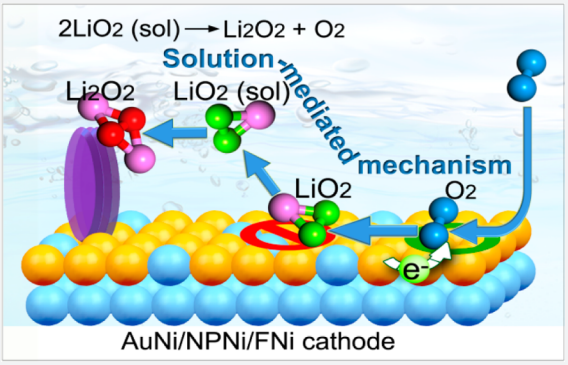

INTRODUCTION

Rechargeable lithium−oxygen (Li−O_2) batteries have received rapidly growing attention because of their high theoretical energy density (3,600 Wh kg^{-1}), their ability to significantly outperform state-of-the-art Li-ion batteries, and their potential as a promising alternative to gasoline.[1−7] Before the potential of Li−O_2 technology can be fully realized, however, a number of important issues must be addressed, such as low round-trip efficiency, low rate capability, and a poor cycle life.[8,9] The primary cause of these problems is the poor electrochemical/chemical stability of the Li−O_2 system, i.e., the highly reactive reduced oxygen species (Li_2O_2 or its intermediate LiO_2) attack the cathode and electrolyte, resulting in the formation and accumulation of undesirable byproducts (e.g., Li_2CO_3) upon cycling that lead to performance degradation and premature battery death.[10,11]

It has been recently recognized that the chemical instability of the battery can be partially overcome by employing a sophisticated cathode, reducing the discharge/charge overpotentials to alleviate electrolyte decomposition,[12,13] and enhancing the electrochemical stability of the cathode to avoid its own decomposition as well as electrolyte decomposition promoted by the cathode.[14−16] Consequently, the stability of the Li−O_2 system depends on the availability of chemically stable cathodes. To date, carbon material has been widely used as a cathode in Li−O_2 batteries.[17−21] The high conductivity, light weight, and rich porous structure of carbon cathodes endow the Li−O_2 batteries with a high specific capacity and superior rate capability. However, carbon cathodes are unstable in the presence of Li_2O_2 and/or LiO_2 upon charging above 3.5 V, and carbon actively catalyzes electrolyte decomposition upon discharge and charge, resulting in poor cycle stability of the Li−O_2 batteries and rendering carbon cathodes unsuitable for these batteries.[22−24] This problem can be solved in principle by replacing carbon with other noncarbonaceous cathode materials. Very few suitable materials, including noble metals,[25] metal oxides,[26] metal carbide,[27] MoS_2,[28] Ru/$TiSi_2$,[29] CoO_x/Co,[30] Pt/Co_3O_4,[31] and RuO_2/NiO,[32] have been used in cathodes to date. Although progress has been achieved regarding battery stability, the use of these noncarbonaceous cathodes has some disadvantages. All noble metals are expensive and difficult to fabricate as a cathode. Most metal oxides suffer from low electrical conductivity. Especially, the high mass and small surface area of these noncarbonaceous cathodes destroy the key advantage of high specific capacity offered by Li−O_2 batteries (typically less than 3000 mAh g^{-1} even based on the weight of the catalyst). Designing a porous cathode that simultaneously achieves a high chemical stability and a superior electrochemical performance remains a daunting challenge.

With the above understanding in mind, we speculate that a porous metal material coated with a noble metal in the cathode should offer many advantages, such as (1) high chemical

Received: March 17, 2017
Published: May 24, 2017

DOI: 10.1021/acscentsci.7b00120
ACS Cent. Sci. 2017, 3, 598−604

stability against the harsh and aggressive environment in Li−O_2 batteries, (2) a combination of the good catalytic activity of noble metals and the high conductivity of base metal materials, and (3) preservation of the initial nanoporous structure of the base metal materials with a high specific surface area to ensure rich catalytic active sites, fast mass transfer, and abundant void space to house the generated discharge products. To this end, we first report the design of nanoporous Ni with a nanoengineered AuNi alloy surface directly attached to Ni foam (AuNi/NPNi/FNi) as a new all-metal cathode system. Highly porous NPNi/FNi or FNi acts only as an effective current collector that provides good electron transport, fast mass transfer, and sufficient void volume to house the generated discharge product Li_2O_2. The ultrathin AuNi alloy overlayer attached to the surface acts as an effective electrocatalyst that promotes the formation and decomposition of Li_2O_2. The all-metal cathode design excludes the side reactions involving carbon. This cathode demonstrates the reversible formation and decomposition of Li_2O_2 and has relatively low overpotentials, ultrahigh specific capacity, and high cycle stability due to its unique design in both structure and component; the values of these properties are many times higher than those of the noncarbonaceous cathodes previously reported.[25−32]

RESULTS AND DISCUSSION

Structural Analysis of the AuNi/NPNi/FNi Cathode. Figure S1 schematically illustrates the synthesis strategy for the AuNi/NPNi/FNi cathode. First, sheet-like nanoporous Ni (NPNi) is deposited and the tips are attached to the framework of Ni foam (FNi) using the rapid decomposition of a metal complex with thermal treatment. Then, an adequate amount of Au is deposited in situ uniformly onto the surface of the NPNi/FNi (Au/NPNi/FNi) by redox replacement of $AuCl_4^-$, where the morphology and amount of deposited Au can be effectively controlled by maintaining a constant temperature, concentration, and/or time of replacement reaction. Finally, the AuNi alloy with 15 atom % Ni is formed by rapid atom interdiffusion between the Au overlayer and the NPNi/FNi surface at elevated temperatures (AuNi/NPNi/FNi). The morphology and porous structure of the AuNi/NPNi/FNi cathode are investigated using field emission scanning electron microscopy (SEM) and transmission electron microscopy (TEM). As shown in Figures 1a and 1b, without the help of any additional binder or solvent, the tips of AuNi/NPNi are attached to the framework of the Ni foam, while the large pores of the Ni foam are kept intact, which ensures the formation of a free-standing structure and a favorable low-resistance pathway for electron transfer. Even after the cathode is subjected to strong ultrasound for 1 h (frequency of 40 kHz, power of 200 W), no AuNi or AuNi/NPNi is removed from the FNi, indicating the superior mechanical stability of the AuNi/NPNi/FNi cathode (Figure 1c). A high-magnification observation (Figure 1d) of the AuNi/NPNi/FNi cathode reveals that AuNi/NPNi consists of fully developed and well-connected 3D macropores with a wide size range (500 nm to 3.0 μm). The low-magnification TEM image (Figure 1e) further illustrates the highly porous nature of AuNi/NPNi. From the pore-size distribution (inset in Figure 1f), two types of pores are clearly observed, micropores (~3−4 nm) and mesopores, with a wide size range (~5−100 nm), which is in agreement with the TEM results (Figure 1e). The highly porous structure of AuNi/NPNi offers a high specific area of 20.29 $m^2\ g^{-1}_{AuNi/NPNi}$, which is

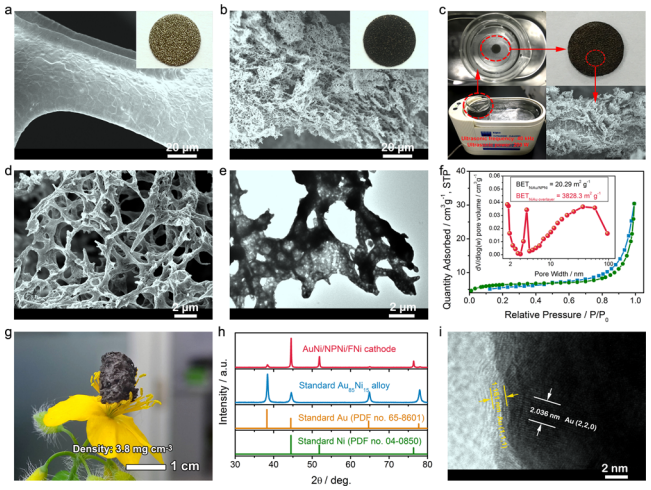

Figure 1. Structure of the cathode. (a) Field emission scanning electron microscopic (FESEM) image and photograph (inset) of the pristine FNi. (b) FESEM image and photograph (inset) of the as-prepared AuNi/NPNi/FNi cathode. (c) Morphology of the AuNi/NPNi/FNi cathode after ultrasonic processing. (d) Enlarged image of b. (e) TEM image of the AuNi/NPNi. (f) Nitrogen adsorption−desorption isotherms and pore-size distribution (inset) of AuNi/NPNi. (g) Black AuNi/NPNi on stamen. (h) X-ray diffraction patterns of the AuNi/NPNi/FNi cathode and the patterns of the as-prepared $Au_{85}Ni_{15}$ alloy. The patterns for standard Au and Ni are also shown for reference. (i) Enlarged image of e. NPNi is covered with a AuNi alloy overlayer with a thickness of 2.1 nm.

confirmed by the nitrogen absorption−desorption isotherms (Figure 1f). Based on the inductively coupled plasma optical emission spectrometry (ICP-OES) result (the weight ratio of AuNi to AuNi/NPNi is 0.53 atom %, Table S1), the calculated specific area of the AuNi overlayer is 3828.3 $m^2\ g^{-1}_{AuNi}$, which offers a large cathode−electrolyte contact area to ensure high availability of the catalytic active sites in the Li−O_2 cell. Furthermore, the highly porous nature of metallic AuNi/NPNi results in an ultralow density (ρ = 3.8 mg cm^{-3}), which is comparable to that of carbon aerogels ($\rho \geq$ 2.0 mg cm^{-3})[33,34] and lower than that of other ultralight materials ($\rho \geq$ 8.0 mg cm^{-3})[35−37] (Figure 1g). The powder X-ray diffraction (PXRD) analysis of AuNi/NPNi/FNi (Figure 1h) reveals that the diffraction peaks can be indexed to well-crystallized Au (PDF No. 65-8601) and $Au_{85}Ni_{15}$ alloy. The high-magnification TEM image reveals that the NPNi surface is well-covered by the AuNi overlayer with a thickness of ~2.1 nm (Figure 1i and Figure S2). This thickness and constitution of the AuNi alloy were determined by continuously optimized experimental results (Figures S3, S4, and S5). This unique all-metal AuNi/NPNi/FNi cathode with a nanoengineered AuNi surface simultaneously fulfills five key requirements for use as a Li−O_2 battery cathode: good catalytic activity endowed by the AuNi alloy surface, highly porous structure endowed by NPNi/FNi, high mechanical stability endowed by the free-standing structure, good conductivity, and, especially, high chemical stability. All of these advantages are beneficial for the electrochemical performance of the Li−O_2 batteries.

Electrochemical Properties of the AuNi/NPNi/FNi Cathode. The electrochemical properties of the AuNi/NPNi/FNi cathode were then examined in a Li−O_2 cell. The FNi, NPNi/FNi, AuNi/FNi, and AuNi/NPNi cathodes (prepared using a similar process to that used for AuNi/NPNi/FNi in the absence of FNi) adhered onto FNi by the

DOI: 10.1021/acscentsci.7b00120
ACS Cent. Sci. 2017, 3, 598−604

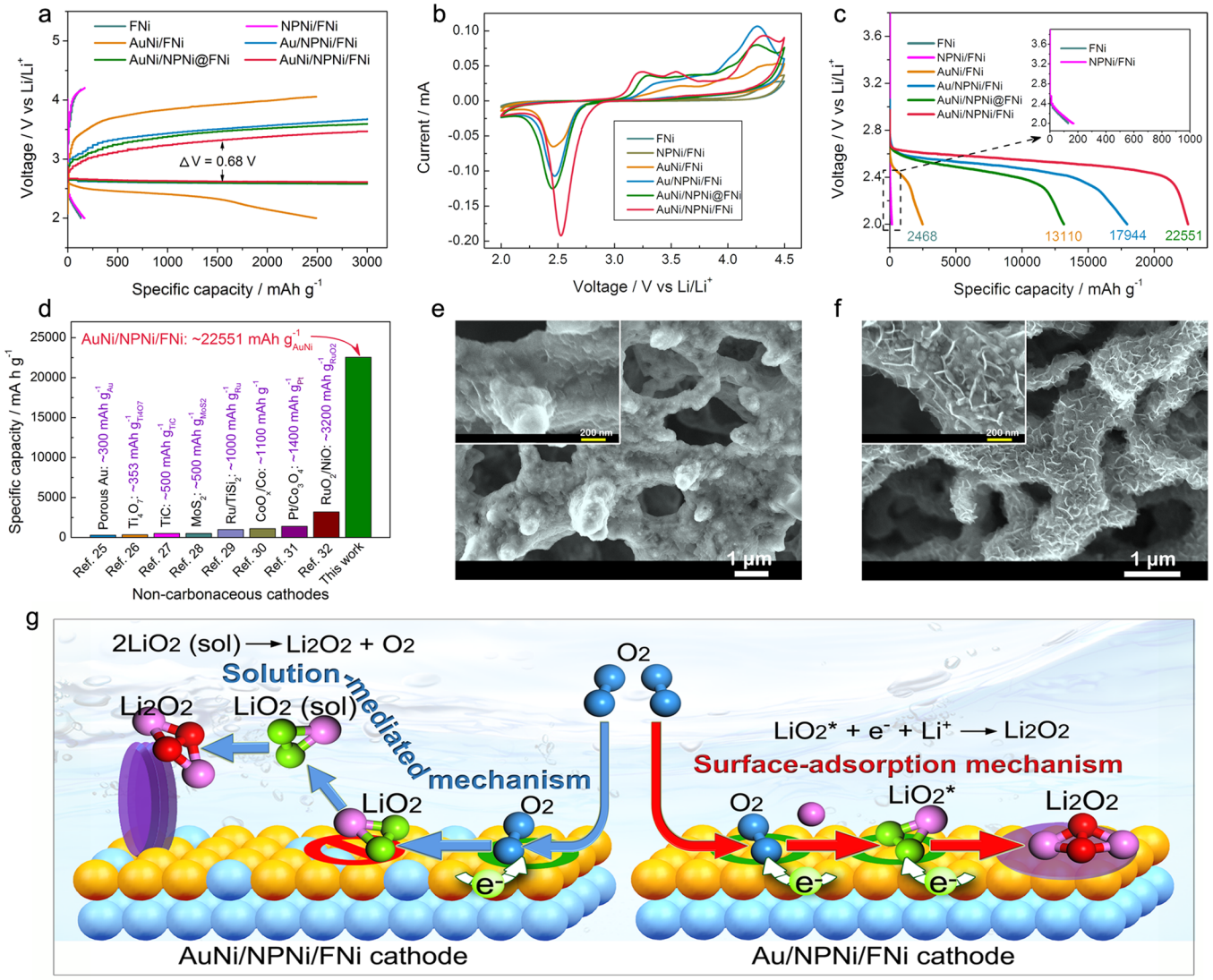

Figure 2. Electrochemical performance. (a) First charge−discharge curves of lithium−oxygen ($Li-O_2$) cells with the six types of cathodes at a current density of 1.0 A g^{-1} and a specific capacity limit of 3,000 mAh g^{-1}. (b) CV of the six types of cathodes in $Li-O_2$ cells at a constant scan rate of 0.05 mV s^{-1}. (c) The rate capability of the $Li-O_2$ cells at the current density of 1.0 A g^{-1}. Inset in c is the enlarged discharge profile of the $Li-O_2$ cells with FNi and NPNi/FNi cathodes. (d) Comparison of the specific capacities of some noncarbonaceous cathodes previously reported. (e) FESEM images of the discharged Au/NPNi/FNi cathode when the discharge capacity is limited to 3,000 mAh g^{-1}. (f) FESEM images of the discharged AuNi/NPNi/FNi cathode. Insets of e and f show the corresponding enlarged FESEM images. (g) A mechanism of electrochemical growth of the film-like and nanosheet-like Li_2O_2.

binder Nafion (AuNi/NPNi@FNi) and the Au/NPNi/FNi cathode were employed for comparison (Figures S6 and S7). Figure 2a shows the first discharge−charge voltage profiles of the $Li-O_2$ cells with the FNi, NPNi/FNi, AuNi/FNi, AuNi/NPNi@FNi, Au/NPNi/FNi, and AuNi/NPNi/FNi cathodes at a current density of 1.0 A g^{-1}. There is almost no discharge/charge voltage platform of the $Li-O_2$ cells using the FNi and NPNi/FNi cathodes, indicating that FNi and NPNi/FNi do not have catalytic activity in the cell. Therefore, porous NPNi/FNi or FNi acts only as an effective current collector that provides good electron transport, fast mass transfer, and sufficient void volume to house the generated discharge products Li_2O_2. The ultrathin Au or AuNi alloy overlayer attached to the surface acts as an effective electrocatalyst that promotes the formation and decomposition of Li_2O_2. Note that the discharge and charge voltage of the $Li-O_2$ cell can be significantly improved with the help of the AuNi/NPNi/FNi cathode, which enhances the round-trip efficiency that is vital for electrochemical energy storage devices. In detail, the discharge voltage of the $Li-O_2$ cell with a AuNi/NPNi/FNi cathode is higher than that with AuNi/NPNi@FNi and Au/NPNi/FNi cathodes by ∼30 mV; its charge voltage is much lower than that with the AuNi/NPNi@FNi cathode by 140 mV and that with the Au/NPNi/FNi by 200 mV. This result is further supported by the oxidation of the artificially Li_2O_2-loaded cathodes in $Li-O_2$ cells, indicating that a similar reduction in the oxidation potential is obtained (Figure S8 and details). The electrochemical processes of oxygen in the $Li-O_2$ cell were also investigated using cyclic voltammetry (CV). Figure 2b presents the CV response of the cells at a constant scan rate of 0.05 mV s^{-1}. The cycle curve reveals that the AuNi/NPNi/FNi cathode exhibits a higher oxygen reduction (ORR) onset potential, a lower evolution reaction (OER) onset potential, and a higher ORR/OER peak current compared with

DOI: 10.1021/acscentsci.7b00120
ACS Cent. Sci. 2017, 3, 598−604

those of the other cathodes. These results indicate that AuNi/NPNi/FNi exhibits a superior electrochemical performance toward both the formation and decomposition of the discharge product (Li_2O_2), which might be derived from the synergy of the following advantageous factors: the higher catalytic activity of the AuNi alloy overlayer than that of Au, which is derived from lattice contraction; the large surface area that provides more reaction sites for the ORR and OER; the highly porous nature, which facilitates the continuous oxygen and lithium ion flow into and out of the inner cathode via larger tunnels (Figure S9); and the cathode surface-induced solvation-mediated formation/decomposition mechanism of Li_2O_2 that benefits the ORR and OER reactions (vide infra).

Figure 2c shows the first discharge curves of the Li−O_2 cells with the six types of cathodes at current densities of 1.0 A g^{-1}. The Li−O_2 cell with the AuNi/NPNi/FNi cathode exhibits an ultrahigh discharge capacity of 22,551 mAh g^{-1}_{AuNi}, which is more than 15 times higher than that with the reported noncarbonaceous cathodes (with discharge capacities typically less than 3,000 mAh g^{-1}) (Figure 2d); this is the best capacity reported to date in this field.[25−32] Note that the discharge capacity of the Li−O_2 cell with the FNi and NPNi/FNi cathodes is negligible within the voltage range, which suggests that the discharge capacities of Li−O_2 cells are derived from ORR on Au or on the AuNi alloy overlayer. Similarly, the discharge capacity of the Li−O_2 cell with the AuNi/FNi cathodes is very low (2,468 mAh g^{-1}_{AuNi}), indicating that the highly porous structure and the large specific surface area of NPNi result in the high discharge/charge capacity. This highly porous nature provides sufficient available void volume to house the generated discharge products, resulting in a substantially enhanced discharge capacity. The Li−O_2 cell with the AuNi/NPNi@FNi cathode exhibits a much lower discharge capacity (13,110) than that with the Au/NPNi/FNi cathode (17,944) (Figure 2c), indicating that the free-standing structure promotes the key advantage of the NPNi porous structure, which is consistent with Figure S6. Unexpectedly, even with the same porous structure, the discharge capacity of the Li−O_2 cell with the AuNi/NPNi/FNi cathode is much higher than that with the Au/NPNi/FNi cathode by ∼4,607 mAh g^{-1}. The difference in the specific capacities of the two cathodes is considered to arise from the different deposition behaviors and morphologies of the discharge product. To this end, the morphologies of the two cathodes after discharge were examined. Figures 2e and 2f show the SEM images of the discharged Au/NPNi/FNi and AuNi/NPNi/FNi cathodes at a fixed capacity of 3,000 mAh g^{-1}. After discharge of the cell, the surface of the Au/NPNi/FNi cathode was almost fully covered by film-like discharge products (Figure 2e), which inevitably impedes oxygen, lithium-ion, and charge transfer within the cathode during subsequent discharge, resulting in severe polarization and premature finishing of the discharge process, causing low capacities and high overpotential. In sharp contrast, the nanosheet-like discharge products are uniformly and loosely dispersed onto the surface of the AuNi/NPNi/FNi cathode (Figure 2f); this arrangement helps maintain active sites for the ORR on the cathode, supporting the electrochemical reaction during subsequent discharge and leading to high capacities of the Li−O_2 cell. PXRD analysis of the discharged cathodes confirmed that Li_2O_2 is the only crystalline product in the two cases, regardless of the difference in morphology (Figure S10). We argue that the difference in morphology of the two discharge processes arises from an elevated solution-mediated mechanism for Li_2O_2 formation that overcomes the charge transport limitations inherent in the surface growth of Li_2O_2.[38] Figure 2g schematically shows the feasible mechanisms of electrochemical growth of the film-like and nanosheet-like Li_2O_2. First, O_2 undergoes a one-electron reduction to O_2^- on the ORR site of two cathodes. On the Au/NPNi/FNi cathode, the superoxide species (O_2^-* and/or LiO_2*, where * indicates surface-adsorbed O_2^- and LiO_2) adsorb onto the cathode surface and undergo a second reduction on the neighboring ORR site of Au, immediately forming Li_2O_2 thin films on the cathode surface. In contrast, on the AuNi/NPNi/FNi cathode, the continuous ORR site of Au is severed by the presence of the Ni atom, which prevents the second reduction of the superoxide species and promotes their diffusion into the electrolyte, forming dissolved solvates of superoxide species (LiO_2(sol) and/or O_2^-(sol)). The dissolved species undergo disproportionation, ultimately forming large Li_2O_2 nanosheet-like crystals. However, in a real system, Li_2O_2 growth is more complicated, and further studies using a combination of electrochemical and theoretical approaches are in progress to elucidate the exact functions of the AuNi/NPNi/FNi cathode.

Another considerable improvement of the Li−O_2 cell with the AuNi/NPNi/FNi cathode is the cycling stability. These cells were tested with the recently widely used capacity limited cycle method. Figure 3a presents the typical voltage profiles for

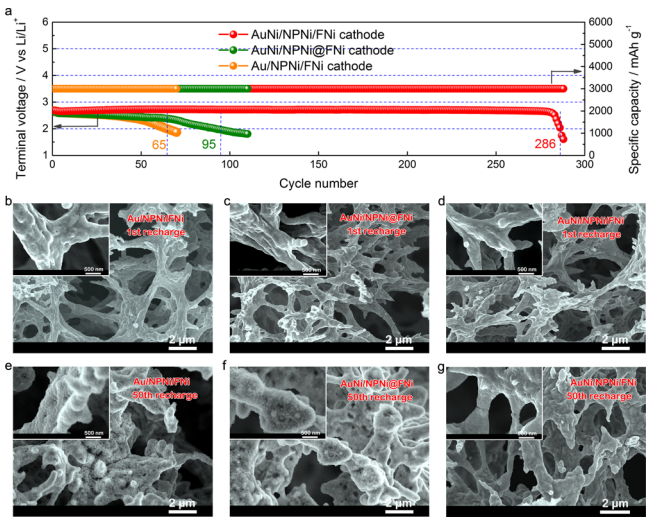

Figure 3. Cathode rechargeability. (a) Variation of the terminal voltage upon the discharge of the Li−O_2 cells with the three types of cathodes at current densities of 1.0 A g^{-1} and a specific capacity limit of 3000 mAh g^{-1}. FESEM images of the recharged (b) Au/NPNi/FNi, (c) AuNi/NPNi@FNi, and (d) AuNi/NPNi/FNi cathodes after the first cycle. FESEM images of the recharged (e) Au/NPNi/FNi, (f) AuNi/NPNi@FNi, and (g) AuNi/NPNi/FNi cathodes after the 50th cycle. Insets of b−g show the corresponding enlarged FESEM images.

Li−O_2 cells with AuNi/NPNi@FNi, Au/NPNi/FNi, and AuNi/NPNi/FNi cathodes cycled at a rate of 1.0 A g^{-1} and with a fixed capacity of 3,000 mAh g^{-1}. The voltage obtained at the discharge terminal of the AuNi/NPNi@FNi cathode in the Li−O_2 cell is >2.0 V for 286 cycles. In contrast, the discharge voltages of the Au/NPNi/FNi and AuNi/NPNi@FNi cathodes degrade to 2.0 V after only 65 and 95 cycles, respectively. This finding confirms that the AuNi/NPNi/FNi cathode has superior rechargeability and cycling stability. To further understand this superior cycling stability, the evolution of the

DOI: 10.1021/acscentsci.7b00120
ACS Cent. Sci. 2017, 3, 598−604

morphology of the three discharged cathodes after the first and 50th cycles was examined. In the AuNi/NPNi/FNi cathode, the platelet-like Li_2O_2 structure disappeared, and the initial nanoporous structure of the whole cathode was almost fully recovered after the first recharge, indicating good reversibility and structural stability of the AuNi/NPNi/FNi cathode (Figure 3d). Even after 50 cycles, the AuNi/NPNi/FNi cathode was only covered by a few small particles (Figure 3g), which can be ascribed to Li_2CO_3, HCO_2Li, or CH_3CO_2Li from the side reactions of the Li_2O_2 and/or intermediates, such as LiO_2*, and electrolyte upon cycling (Figure S13). In contrast, in the Au/NPNi/FNi and AuNi/NPNi@FNi cathodes, massive Li_2CO_3 and lithium carboxylates were packed densely onto the cathode surface (Figures 3e, 3f, and S13). This continuous accumulation of byproducts upon cycling hinders the transport of the superoxide species, electrons, and lithium ions within the cathode during subsequent cycling, consequently leading to the failure of the Li−O_2 cell with these cathodes. We speculate that the superior rechargeability of the AuNi/NPNi/FNi cathode might be derived from the synergy of the following advantageous factors: the structural stability of AuNi/NPNi/FNi helps to maintain stable cathode integrity upon cycling, the free-standing structure of the AuNi/NPNi/FNi cathode can provide a fast electron conduction to the cathode−Li_2O_2 interface, the uniformly and loosely distributed Li_2O_2 nanosheets provide sufficient Li_2O_2−electrolyte interfaces that support the electrochemical reaction during the charge process, and the AuNi/NPNi/FNi cathode significantly alleviates the high-potential-induced electrolyte decomposition during charging by lowering the charge voltage.[12,13]

Electrochemical Stability of the AuNi/NPNi/FNi Cathode. To verify the electrochemical stability of the cathode, undischarged FNi, NPNi/FNi, Au/NPNi/FNi, and AuNi/NPNi/FNi cathodes were also directly subjected to electrochemical oxidation in Li−O_2 cells at a current density of 1.0 A g^{-1} (Figure S14). The Li−O_2 cell with the four all-metal cathodes demonstrated a continuous charge capacity upon charging above 4.2 V, which may be due to the oxidation of the electrolyte and cathode (Figure S14a). PXRD analysis of the four charged cathodes confirmed that there were no peaks for Ni oxides and/or Au oxides, suggesting that the cathodes were not oxidized upon charging (Figures S14b−S14e). Unexpectedly, oxidation of the all-metal cathodes was not observed, even after 50 discharge/recharge cycles (Figure S15). These results confirmed that the four all-metal cathodes have superior electrochemical stability in Li−O_2 cells, which encouraged a further investigation into the electrochemical stability of the Li−O_2 system with the all-metal cathodes. To this end, the parasitic electrochemistry/chemistry in the Li−O_2 cells was examined using quantitative Fourier transform infrared (FTIR) and ^{1}H nuclear magnetic resonance (NMR) spectroscopy (Figure 4). The conventional SP carbon cathode was also employed for comparison (Figure S16). The FTIR spectra indicate that the discharge products in Li−O_2 cells withboth AuNi/NPNi/FNi and SP carbon cathodes after the first discharge are overwhelmingly dominated by Li_2O_2 (Figure 4a). However, after the 40th cycle, FTIR provides clear evidence of significant side reactions on the pristine SP carbon cathode. In addition to Li_2O_2, the peaks at ∼864, 1441, and 1500 cm^{-1} can be assigned to Li_2CO_3, that at ∼1371 cm^{-1} to HCO_2Li, and that at ∼1615 cm^{-1} to CH_3CO_2Li (Figure 4b). In contrast, significantly weaker peaks are ascribed to side products on the AuNi/NPNi/FNi cathode after the 40th

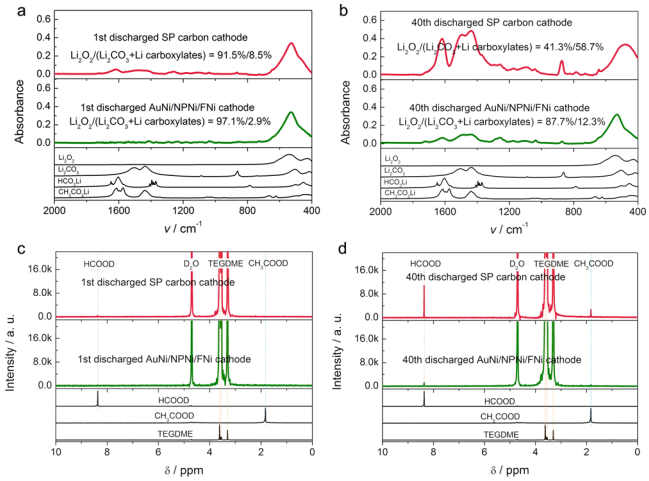

Figure 4. Parasitic electrochemistry/chemistry. FTIR spectra of the conventional SP carbon and AuNi/NPNi/FNi cathodes after (a) the first discharge and (b) the 40th discharge. The spectra for Li_2O_2, Li_2CO_3, HCO_2Li, and CH_3CO_2Li are also shown for reference. ^{1}H NMR spectra of the conventional SP carbon and AuNi/NPNi/FNi cathodes after (c) the first discharge and (d) the 40th discharge. The spectra for TEGDME, HCO_2Li, and CH_3CO_2Li are also shown for reference.

cycle and may have resulted from the partial decomposition of the ether-based electrolyte. Based on the FTIR calibration curves obtained in our recent work[12,38,39] the molar ratio of the Li_2O_2 to the side products (Li_2CO_3, CH_3CO_2Li, and HCO_2Li) was determined using the obtained FTIR spectra (Figures 4a and 4b). In sharp contrast, the Li_2O_2/side product ratio at the end of 40 cycles for the Li−O_2 cell with the SP carbon cathode was only 41.3/58.7, which is much lower than that obtained with the AuNi/NPNi/FNi cathode (87.7/12.3). In addition, ^{1}H NMR spectroscopy (Figures 4c and 4d) indicates that the amount of electrolyte decomposition products (CH_3CO_2Li and HCO_2Li) on the AuNi/NPNi/FNi cathode is much less than that on the SP carbon cathode during cycling, which is consistent with the above FTIR results. These observations clearly demonstrate the superiority of the Li−O_2 cells with the all-metal cathode in terms of the electrochemical/chemical stability, which can be ascribed to the ability of AuNi/NPNi/FNi to effectively avoid the possible side reactions between the conventional carbon defect sites and the Li_2O_2 or between the defect sites and the electrolyte.[22−24] In addition, the low charge potential observed with the all-metal cathode alleviates the high-potential-induced decomposition of the electrolyte during charging, which also contributes to the high electrochemical/chemical stability.[12,13]

■ CONCLUSIONS

In conclusion, the design of a porous cathode that simultaneously achieves a high chemical stability and a superior electrochemical performance remains a daunting challenge. In this work, we first developed nanoporous Ni with a nanoengineered AuNi alloy surface directly attached to Ni foam (AuNi/NPNi/FNi) as a new all-metal cathode system. Compared with the popularly used carbon cathode, the AuNi/NPNi/FNi cathode is advantageous in that it does not show measurable reactivity toward the discharge product (Li_2O_2) and/or the reaction intermediates (LiO_2). The Li−O_2 cell with an all-metal cathode demonstrates the reversible formation and

DOI: 10.1021/acscentsci.7b00120
ACS Cent. Sci. 2017, 3, 598−604

decomposition of Li_2O_2 and relatively low overpotentials, ultrahigh specific capacity, and cycle stability. These superior properties are explained by the enhanced solvation-mediated formation of the discharge products as well as the tailored properties of the all-metal cathode, including intrinsic chemical stability endowed by the metal nature, high specific surface area and the highly porous structure that provide sufficient void volume to house the generated discharge products and fast mass transfer, the high conductivity that enables fast electron transfer from the reaction sites, and superior mechanical stability that helps to maintain stable cathode integrity upon cycling. The results also suggest that both the material and structure of the cathode should be optimized to simultaneously achieve a high chemical stability and a superior electrochemical performance of Li−O_2 batteries.

■ ASSOCIATED CONTENT

Supporting Information

The Supporting Information is available free of charge on the ACS Publications website at DOI: 10.1021/acscentsci.7b00120.

Complete experimental details and supporting figures and tables (PDF)

■ AUTHOR INFORMATION

Corresponding Author

*E-mail: xbzhang@ciac.ac.cn.

ORCID

Xin-Bo Zhang: 0000-0002-5806-159X

Notes

The authors declare no competing financial interest.

■ ACKNOWLEDGMENTS

This workwas financially supported by National Program on Key Basic Research Project of China (2012CB215500 and 2014CB932300), Strategic Priority Research Program of the Chinese Academy of Sciences (Grant No. XDA09010404), Ministry of Science and Technology of the People's Republic of China (Grant No. 2016YFB0100100), Technology and Industry for National Defence of the People's Republic of China (Grant No. JCKY2016130B010), National Natural Science Foundation of China (21422108 and 51472232), and Jilin Province Science and Technology Development Program (Grant No. 20160101289JC).

■ REFERENCES

(1) Gao, X.; Chen, Y.; Johnson, L.; Bruce, P. G. Promoting solution phase discharge in Li−O_2 batteries containing weakly solvating electrolyte solutions. *Nat. Mater.* **2016**, *15*, 882−888.

(2) Liu, T.; Leskes, M.; Yu, W.; Moore, A. J.; Zhou, L.; Bayley, P. M.; Kim, G.; Grey, C. P. Cycling Li−O_2 batteries via LiOH formation and decomposition. *Science* **2015**, *350*, 530−533.

(3) Lu, J.; Lee, Y. J.; Luo, X.; Lau, K. C.; Asadi, M.; Wang, H.; Brombosz, S.; Wen, J.; Zhai, D.; Chen, Z.; Miller, D. J.; Jeong, Y. S.; Park, J.; Fang, Z. Z.; Kumar, B.; Salehi-Khojin, A.; Sun, Y.; Curtiss, L. A.; Amine, K. A lithium−oxygen battery based on lithium superoxide. *Nature* **2016**, *529*, 377−382.

(4) Oh, S. H.; Black, R.; Pomerantseva, E.; Lee, J. H.; Nazar, L. F. Synthesis of a metallic mesoporous pyrochlore as a catalyst for lithium−O_2 battery. *Nat. Chem.* **2012**, *4*, 1004−1010.

(5) Jung, H. G.; Hassoun, J.; Park, J. B.; Sun, Y. K.; Scrosati, B. An improved high-performance lithium−air battery. *Nat. Chem.* **2012**, *4*, 579−585.

(6) Aetukuri, N. B.; McCloskey, B. D.; García, J. M.; Krupp, L. E.; Viswanathan, V.; Luntz, A. C. Solvating additives drive solution-mediated electrochemistry and enhance toroid growth in non-aqueous Li−O_2 batteries. *Nat. Chem.* **2015**, *7*, 50−56.

(7) Johnson, L.; Li, C.; Liu, Z.; Chen, Y.; Freunberger, S. A.; Ashok, P. C.; Praveen, B. B.; Dholakia, K.; Tarascon, J.; Bruce, P. G. The role of LiO_2 solubility in O_2 reduction in aprotic solvents and its consequences for Li−O_2 batteries. *Nat. Chem.* **2014**, *6*, 1091−1099.

(8) Sun, B.; Guo, L.; Ju, Y.; Munroe, P.; Wang, E.; Peng, Z.; Wang, G. Unraveling the catalytic activities of ruthenium nanocrystals in high performance aprotic Li−O_2 batteries. *Nano Energy* **2016**, *28*, 486−494.

(9) Su, D.; Seo, D. H.; Ju, Y.; Han, Z.; Ostrikov, K.; Dou, S.; Ahn, H.-J.; Peng, Z.; Wang, G. Ruthenium nanocrystal decorated vertical graphene nanosheets@Ni foam as highly efficient cathode catalysts for lithium-oxygen batteries. *NPG Asia Mater.* **2016**, *8*, e286.

(10) McCloskey, B. D.; Valery, A.; Luntz, A. C.; Gowda, S. R.; Wallraff, G. M.; Garcia, J. M.; Mori, T.; Krupp, L. E. Combining accurate O_2 and Li_2O_2 assays to separate discharge and charge stability limitations in nonaqueous Li−O_2 batteries. *J. Phys. Chem. Lett.* **2013**, *4*, 2989−2993.

(11) Zhang, T.; Zhou, H. From Li−O_2 to Li−air batteries: carbon nanotubes/ionic liquid gels with a tricontinuous passage of electrons, ions, and oxygen. *Angew. Chem., Int. Ed.* **2012**, *51*, 11062−11067.

(12) Xu, J.-J.; Wang, Z.-L.; Xu, D.; Zhang, L.-L.; Zhang, X.-B. Tailoring deposition and morphology of discharge products towards high-rate and long-life lithium−oxygen batteries. *Nat. Commun.* **2013**, *4*, 2438.

(13) Chang, Z.-W.; Xu, J.-J.; Liu, Q.-C.; Li, L.; Zhang, X.-B. Recent progress on stability enhancement for cathode in rechargeable non-aqueous lithium-oxygen battery. *Adv. Energy Mater.* **2015**, *5*, 1500633.

(14) Jian, Z.; Liu, P.; Li, F.; He, P.; Guo, X.; Chen, M.; Zhou, H. Core−shell-structured CNT@RuO_2 composite as a high-performance cathode catalyst for rechargeable Li−O_2 batteries. *Angew. Chem., Int. Ed.* **2014**, *53*, 442−446.

(15) Lu, J.; Lei, Y.; Lau, K. C.; Luo, X.; Du, P.; Wen, J.; Assary, R. S.; Das, U.; Miller, D. J.; Elam, J. W.; Albishri, H. M.; El-Hady, D. A.; Sun, Y.-K.; Curtiss, L. A.; Amine, K. A nanostructured cathode architecture for low charge overpotential in lithium−oxygen batteries. *Nat. Commun.* **2013**, *4*, 2383.

(16) Xie, J.; Yao, X.; Cheng, Q.; Madden, I. P.; Dornath, P.; Chang, C. C.; Fan, W.; Wang, D. Three dimensionally ordered mesoporous carbon as a stable, high-performance Li−O_2 battery cathode. *Angew. Chem.* **2015**, *127*, 4373−4377.

(17) Guo, Z.; Zhou, D.; Dong, X.; Qiu, Z.; Wang, Y.; Xia, Y. Ordered hierarchical mesoporous/macroporous carbon: a high-performance catalyst for rechargeable Li−O_2 batteries. *Adv. Mater.* **2013**, *25*, 5668−5672.

(18) Lim, H. D.; Park, K. Y.; Song, H.; Jang, E. Y.; Gwon, H.; Kim, J.; Kim, Y. H.; Lima, M. D.; Robles, R. O.; Lepró, X.; Baughman, R. H.; Kang, K. Enhanced power and rechargeability of a Li−O_2 battery based on a hierarchical-fibril CNT electrode. *Adv. Mater.* **2013**, *25*, 1348−1352.

(19) Sun, B.; Huang, X.; Chen, S.; Munroe, P.; Wang, G. Porous graphene nanoarchitectures: An efficient catalyst for low charge-overpotential, long life, and high capacity lithium-oxygen batteries. *Nano Lett.* **2014**, *14*, 3145−3152.

(20) Oh, D.; Qi, J.; Lu, Y. C.; Zhang, Y.; Shao-Horn, Y.; Belcher, A. M. Biologically enhanced cathode design for improved capacity and cycle life for lithium-oxygen batteries. *Nat. Commun.* **2013**, *4*, 2756.

(21) Xu, J.-J.; Xu, D.; Wang, Z.-L.; Wang, H.-G.; Zhang, L.-L.; Zhang, X.-B. Synthesis of perovskite-based porous $La_{0.75}Sr_{0.25}MnO_3$ nanotubes as a highly efficient electrocatalyst for rechargeable lithium−oxygen batteries. *Angew. Chem., Int. Ed.* **2013**, *52*, 3887−3890.

(22) McCloskey, B. D.; Speidel, A.; Scheffler, R.; Miller, D. C.; Viswanathan, V.; Hummelshøj, J. S.; Nørskov, J. K.; Luntz, A. C. Twin problems of interfacial carbonate formation in nonaqueous Li−O_2 batteries. *J. Phys. Chem. Lett.* **2012**, *3*, 997−1001.

DOI: 10.1021/acscentsci.7b00120
ACS Cent. Sci. 2017, 3, 598−604

(23) Ottakam Thotiyl, M. M.; Freunberger, S. A.; Peng, Z.; Bruce, P. G. The carbon electrode in nonaqueous Li−O_2 cells. *J. Am. Chem. Soc.* **2013**, *135*, 494−500.
(24) Itkis, D. M.; Semenenko, D. A.; Kataev, E. Y.; Belova, A. I.; Neudachina, V. S.; Sirotina, A. P.; Hävecker, M.; Teschner, D.; Knop-Gericke, A.; Dudin, P.; Barinov, A.; Goodilin, E. A.; Shao-Horn, Y.; Yashina, L. V. Reactivity of carbon in lithium−oxygen battery positive electrodes. *Nano Lett.* **2013**, *13*, 4697−4701.
(25) Peng, Z.; Freunberger, S.; Chen, Y.; Bruce, P. G. A reversible and higher-rate Li−O_2 battery. *Science* **2012**, *337*, 563−566.
(26) Kundu, D.; Black, R.; Berg, E. J.; Nazar, L. F. A highly active nanostructured metallic oxide cathode for aprotic Li−O_2 batteries. *Energy Environ. Sci.* **2015**, *8*, 1292−1298.
(27) Thotiyl, M. M. O.; Freunberger, S. A.; Peng, Z.; Chen, Y.; Liu, Z.; Bruce, P. G. A stable cathode for the aprotic Li−O_2 battery. *Nat. Mater.* **2013**, *12*, 1050−1056.
(28) Asadi, M.; Kumar, B.; Liu, C.; Phillips, P.; Yasaei, P.; Behranginia, A.; Zapol, P.; Klie, R. F.; Curtiss, L. A.; Salehi-Khojin, A. Cathode based on molybdenum disulfide nanoflakes for lithium−oxygen batteries. *ACS Nano* **2016**, *10*, 2167−2175.
(29) Xie, J.; Yao, X.; Madden, I. P.; Jiang, D. E.; Chou, L. Y.; Tsung, C. K.; Wang, D. Selective Deposition of Ru nanoparticles on $TiSi_2$ nanonet and its utilization for Li_2O_2 formation and decomposition. *J. Am. Chem. Soc.* **2014**, *136*, 8903−8906.
(30) Shen, C.; Wen, Z.; Wang, F.; Wu, T.; Wu, X. Cobalt-metal-based cathode for lithium−oxygen battery with improved electrochemical performance. *ACS Catal.* **2016**, *6*, 4149−4153.
(31) Cao, J.; Liu, S.; Xie, J.; Zhang, S.; Cao, G.; Zhao, X. Tips-bundled Pt/Co_3O_4 nanowires with directed peripheral growth of Li_2O_2 as efficient binder/carbon-free catalytic cathode for lithium−oxygen Battery. *ACS Catal.* **2015**, *5*, 241−245.
(32) Tan, P.; Wei, Z. H.; Shyy, W.; Zhao, T. S.; Zhu, X. B. A nano-structured RuO_2/NiO cathode enables the operation of non-aqueous lithium−air batteries in ambient air. *Energy Environ. Sci.* **2016**, *9*, 1783−1793.
(33) Zou, J.; Liu, J.; Karakoti, A. S.; Kumar, A.; Joung, D.; Li, Q.; Khondaker, S. I.; Seal, S.; Zhai, L. Ultralight multiwalled carbon nanotube aerogel. *ACS Nano* **2010**, *4*, 7293−7302.
(34) Mecklenburg, M.; Schuchardt, A.; Mishra, Y. K.; Kaps, S.; Adelung, R.; Lotnyk, A.; Kienle, L.; Schulte, K. Aerographite: Ultra lightweight, flexible nanowall, carbon microtube material with outstanding mechanical performance. *Adv. Mater.* **2012**, *24*, 3486−3490.
(35) Verdooren, A.; Chan, H. M.; Grenestedt, J. L.; Harmer, M. P.; Caram, H. S. Fabrication of low-d ensity ferrous metallic foams by reduction of chemically bonded ceramic foams. *J. Am. Ceram. Soc.* **2006**, *89*, 3101−3106.
(36) Tappan, B. C.; Huynh, M. H.; Hiskey, M. A.; Chavez, D. E.; Luther, E. P.; Mang, J. T.; Son, S. F. Ultralow-density nanostructured metal foams: combustion synthesis, morphology, and composition. *J. Am. Chem. Soc.* **2006**, *128*, 6589−5694.
(37) Biener, M. M.; Ye, J.; Baumann, T. F.; Wang, Y. M.; Shin, S. J.; Biener, J.; Hamza, A. V. Ultra-strong and low-density nanotubular bulk materials with tunable feature sizes. *Adv. Mater.* **2014**, *26*, 4808−4813.
(38) Xu, J.-J.; Chang, Z.-W.; Wang, Y.; Liu, D.-P.; Zhang, Y.; Zhang, X.-B. Cathode surface-induced, solvation-mediated, micrometer-sized Li_2O_2 cycling for Li−O_2 batteries. *Adv. Mater.* **2016**, *28*, 9620−9628.
(39) Xu, J.-J.; Wang, Z.-L.; Xu, D.; Meng, F.-Z; Zhang, X.-B. 3D ordered macroporous $LaFeO_3$ as efficient electrocatalyst for Li−O_2 batteries with enhanced rate capability and cyclic performance. *Energy Environ. Sci.* **2014**, *7*, 2213−2219.

DOI: 10.1021/acscentsci.7b00120
ACS Cent. Sci. 2017, 3, 598−604